Five Cytochrome 'Nanowires' Suffice for Prokaryotes to Breathe Rocks Microns Away

Matthew J. Guberman-Pfeffer[a,b,c,*]

Department of Chemistry and Biochemistry, Baylor University, One Bear Place #97348, Waco, Texas 76706, United States

**** Author to whom correspondence should be addressed.***

E-mail: Matthew_Guberman-Pfe@baylor.edu

KEYWORDS: multi-heme, cytochrome, nanowire, redox, conductivity, QM/MM, Geobacter, OmcS

Abstract

Micron-scale electron transfer through polymeric cytochrome 'nanowires' powers prokaryotic life from hydrothermal vents to terrestrial soils in ways not fully understood. Herein, six reduction potentials from recently reported spectroelectrochemistry are each assigned with chemical accuracy (<0.05 eV) to the cryogenic electron microscopy structure of the hexa-heme homopolymeric outer-membrane cytochrome type S (OmcS) from *Geobacter sulfurreducens* using hybrid quantum/classical computations. The unambiguous assignments define a bumpy but overall thermoneutral free energy landscape that is dynamically modulated by <0.1 V under the flow of electrons via redox cooperativities between adjacent hemes. A physiologically relevant ≥5 filaments are predicted to suffice for cellular respiration by pairing, in the context of non-adiabatic Marcus theory, the free energy landscape with reorganization energies that empirically account for protein-water electronic polarizability, and electronic couplings characteristic of the highly conserved heme packing motifs. General considerations on protein electron transfer and comparison to all known cytochrome 'nanowires' suggest the mechanistic insights are broadly applicable to multi-heme cytochromes in all kingdoms of life.

Introduction

Prokaryotes from hydrothermal vents to terrestrial soils can exhale >10^5 electrons/s/cell (>10 fA/cell)[1-3] through filamentous cytochrome 'nanowires'[4] that electrify microbial communities[5] and biotic-abiotic interfaces.[6] This 'rock breathing' strategy for anaerobic life, known as extracellular electron transfer, is ancient,[7] ubiquitous,[8, 9] environmentally significant,[10-13] and holds promise for sustainable technologies,[14-21] but only if its mechanistic underpinnings are elucidated. A fundamental question beyond the limits of current experimental techniques[4, 22-24] that is addressed herein by hybrid quantum/classical computations is: What is the electron transfer mechanism that connects the atomic structures of filamentous cytochromes to their physiological role as mesoscopic electrical conductors?

All known cytochrome filaments[4, 25-28] have the basic anatomy summarized in Figure 1. A single type of cofactor—a bis-histidine ligated *c*-type heme—is repeated hundreds of times and stacked in highly conserved geometries[4] to form a micron-long (linear or branched) spiraling chain, which is encased by a mostly unstructured (≥50% turns and loops) protein sheath. Each filament is constructed of a different Lego-like multi-heme cytochrome that self-polymerizes either exclusively through non-covalent interactions, or one or more coordination bonds between protomers. These filaments attest to the great lengths, biosynthetically and literally, life will go to breathe.

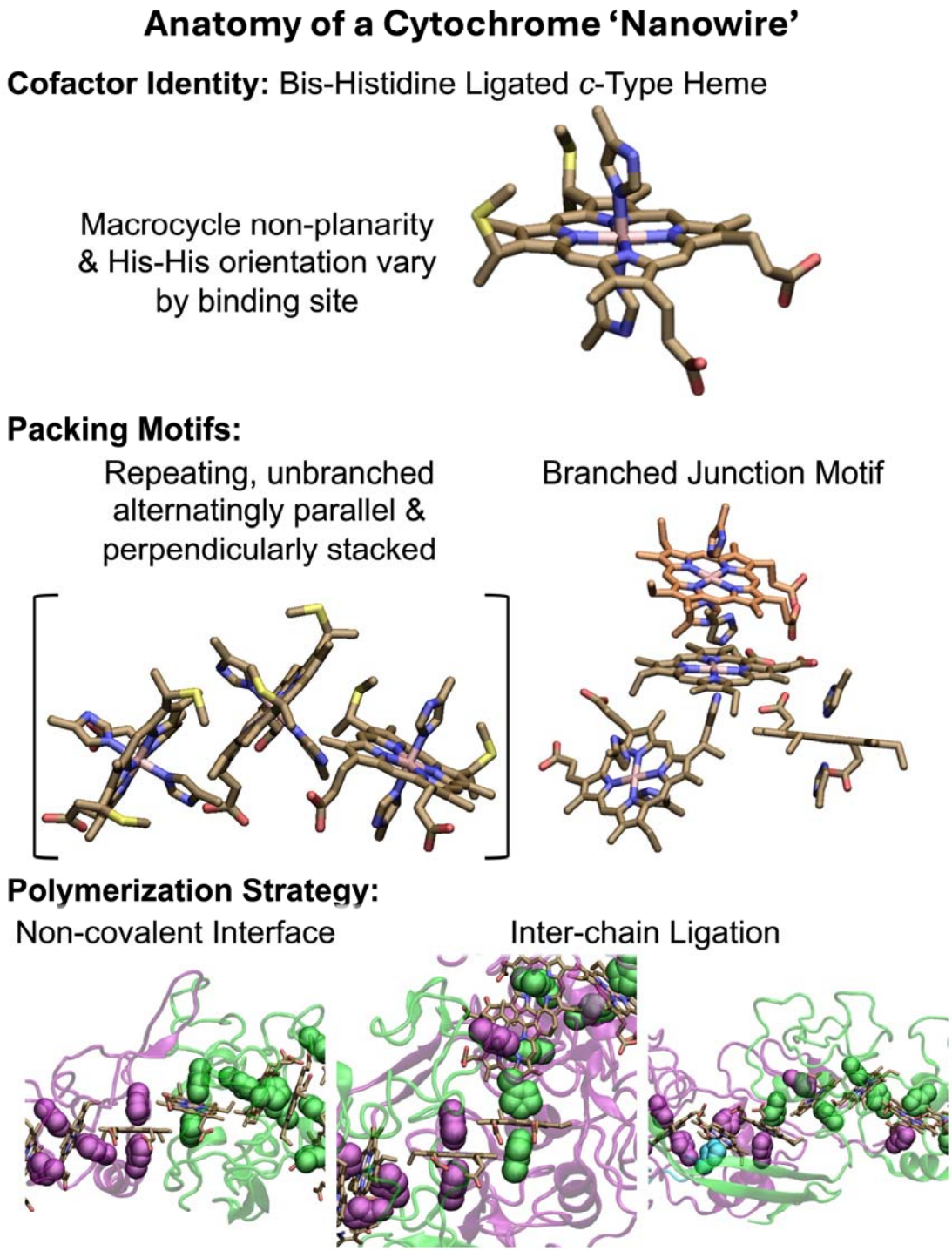

Figure 1. Anatomy of a cytochrome 'nanowire.' The heme cofactor, its packing motifs, and filament polymerization strategies are shown. Purple, green, and cyan indicate different protein chains. His ligands are shown in vdW representation. A heme that is coordinated by two differently colored His ligands receives one of them from the adjacent protein chain. The subunit interfaces shown at the bottom from left to right come from OmcZ (PDB 7LQ5),[28] OmcS (PDB 6EF8),[26] and F2KMU8 (PDB 8E5G).[4] The figure was designed with VMD version 1.9.4a57.[29]

The first-discovered and most extensively characterized representative of the structural class to date is the outer-membrane cytochrome type S (OmcS) from *Geobacter sulfurreducens*.[25, 26, 30] OmcS is a hexa-heme cytochrome that has only ~19% regular 2° structure and self-polymerizes by donating a coordinating His ligand to the penultimate heme of another OmcS molecule.[26]

Theoretical models spanning the entire continuum of electron transfer theory[30-36] have been proposed to describe the function of OmcS since its structure was resolved in 2019.[25, 26] None of these models, however, have successfully linked the atomistic structure to a functional characterization or physiological role. Regardless of whether micron-scale electron transfer is pictured as a relay of reduction-oxidation (redox) reactions between individual (purely incoherent transfer) or blocks of (coherence-assisted transfer) hemes,[30-34] or quantum transport through electronic bands,[35, 36] the models have failed to explain the electronic conductivity measured by atomic force microscopy (AFM);[30] a discrepancy all the more striking since OmcS is 10^3-fold less conductive than another cytochrome filament by the same technique.[37]

The discrepancy is customarily interpreted as a failure of theory.[31, 35] But concerns recently raised about structural and electronic artifacts of the experimental conditions[22] may suggest the comparison is not appropriate. By instead comparing to the metabolic flux of electrons from a *G. sulfurreducens* cell, it is herein demonstrated a relay of redox reactions is physiologically sufficient if, as observed,[38] ≥5 filament/cell are expressed. The redox conductivity model is based on quantum mechanical/molecular mechanical computations at molecular dynamics generated configurations (QM/MM@MD)[33] that are shown to have predicted, within chemical accuracy (<0.05 eV), each of the six redox potentials of the hemes in OmcS 15-months before they were reported by spectroelectrochemistry. General considerations are discussed that

indicate the method, model, and mechanistic insights are applicable to multi-heme chains in all kingdoms of life.

Results and Discussion

Computations Accurately Predict the Measured Spectroelectrochemical Titration Curve

To assess whether the picture of consecutive redox reactions is mechanistically viable for micron-scale electron transfer before resorting to competing alternatives like coherence-assisted charge hopping[31] or decoherent quantum transport,[35, 36] a faithful reproduction of the redox properties of OmcS is mandatory. Figure 2 therefore compares, for the first time, previously published simulated[30, 33] and measured[24] spectroelectrochemical profiles for OmcS.

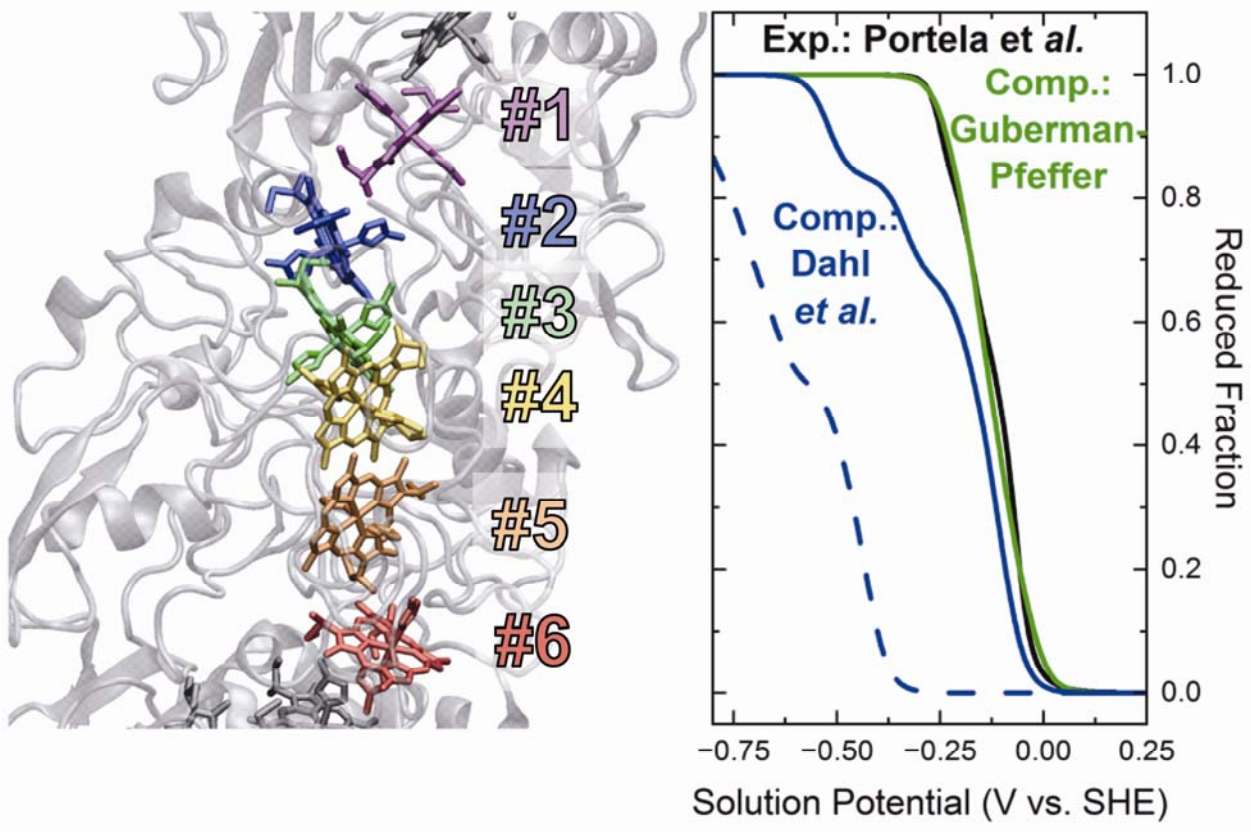

Figure 2. Starting from only the structure of OmcS, quantum mechanical/molecular mechanical computations at molecular dynamics-generated configurations (QM/MM@MD) can accurately reproduce the experimental spectroelectrochemical titration curve. The structure is from PDB 6EF8.[26] The six hemes in the N- to C-terminal direction are numbered sequentially and colored purple, blue, yellow, orange, green and red. The experimental titration curve is reproduced from Portela *et al.*[24] The computed titration curves are simulated from redox potentials reported by Guberman-Pfeffer[33] and Dahl *et al.*[30]

The figure shows the fraction of reduced hemes in the OmcS filament as a function of the solution potential. The blue, green and black solid-line titration curves are respectively and chronologically the redox profiles computationally predicted by Dahl *et al.*,[30] Guberman-Pfeffer,[33] and measured using spectroelectrochemistry by Portela *et al.*[24] The computed solid-line titration curves represent an approximation to a cathodic electrochemical sweep in which each heme was separately reduced while all other hemes were held in the oxidized state. The blue dashed-line titration curve represents an anodic electrochemical sweep simulated by Dahl *et al.*[30] in which each heme was separately oxidized while all other hemes were fixed in the reduced state.

The experimental midpoint potential is -0.132 V vs. Standard Hydrogen Electrode (SHE), which is well reproduced by the QM/MM@MD modeling of Guberman-Pfeffer (-0.116 V vs. SHE) and the cathodic, but not the anodic sweep predicted by Dahl *et al.* (-0.168 and -0.572 V vs. SHE respectively). The enormous and erroneously predicted hysteresis by Dahl *et al.* was previously used to explain why OmcS is six-fold more conductive in the fully reduced versus fully oxidized state, an observation that itself is inconsistent with the nature of a cytochrome. Redox conduction through a cytochrome is maximal when there is an equal proportion of reduced (electron donating) and oxidized (electron accepting) hemes, and rapidly falls to zero when all hemes are either reduced or oxidized.[39]

Spectroelectrochemical Potentials are Assigned to the CryoEM structure with Chemical Accuracy Using a Computational 'Rosette Stone'

Further insight is possible by approximating the spectroelectrochemical titration curve in Figure 2 by a sum of Nernst equations to obtain the potentials for discrete redox transitions that were too finely spaced to be resolved experimentally.[40] There must be as many one-electron

Nernst equations in the sum as there are one-electron redox centers in the protein. A subunit of OmcS has six one-electron donating/accepting heme groups. If the redox profile of a subunit does not depend on its position in the helical pitch of the filament (~4 subunits/pitch), a minimum of six Nernst equations is needed to approximate the titration curve in Figure 2.

Each of these Nernst equations describes a transition between macroscopic redox states (macrostates) in which OmcS gains/losses a single reducing equivalent. As shown in Figure 3, each macrostate (S0 – S6) comprises an ensemble of microstates that describes all the permutations for distributing the reducing equivalences among the six hemes at that macroscopic reduction stage. Sequential addition of six electrons takes OmcS from the fully oxidized (S0) to fully reduced (S6) macrostate, with the number of microstates at each reduction stage following Pascale's triangle (Figure 3). The redox potential of each microstate, weighted by its fractional occupancy among the other microstates for that reduction stage, determines the macroscopic redox potentials obtained by fitting six Nernst equations to the titration curve in Figure 2.

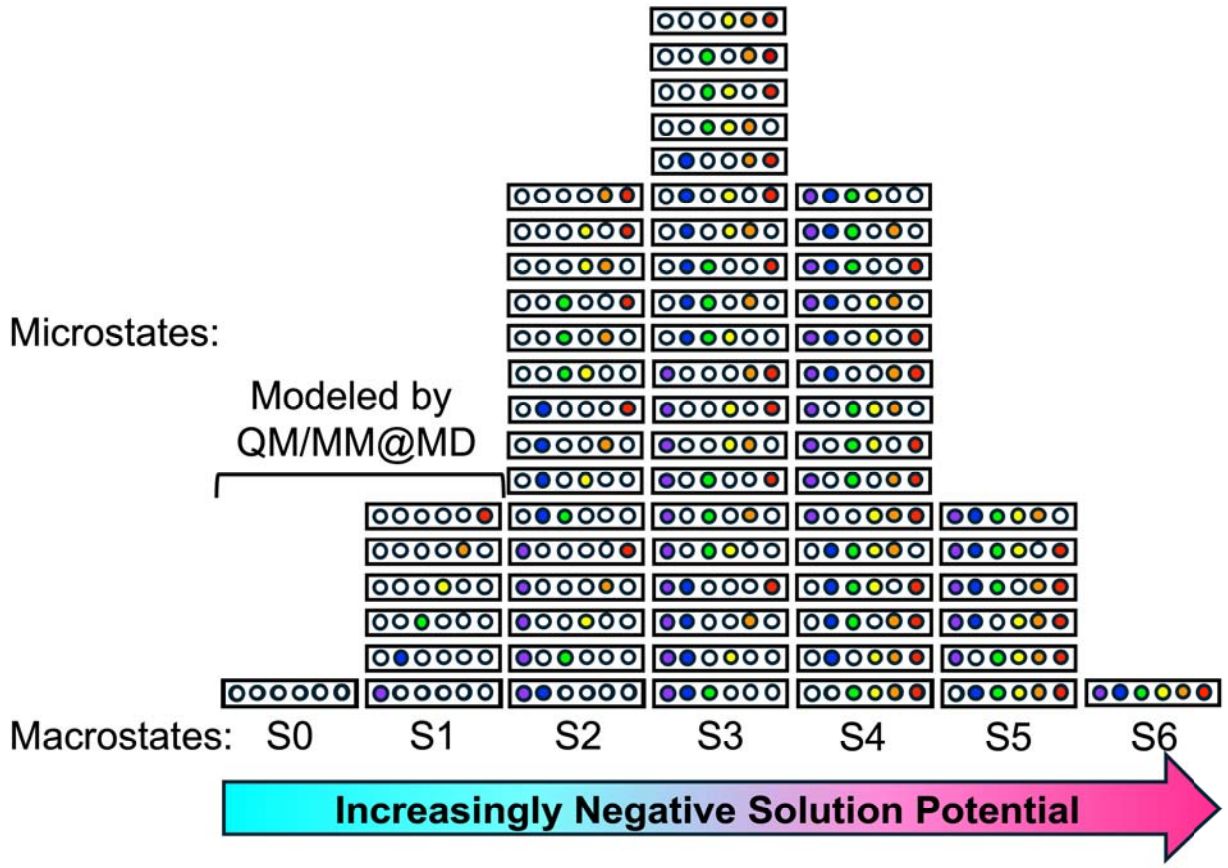

Figure 3. Under increasing negative solution potentials, OmcS passes from the fully oxidized to fully reduced redox macrostate (S0 S6 columns), with the sequentially added reducing equivalence distributed among the hemes in various microstates (rectangles). Each circle represents a heme. Purple, blue, green, yellow, orange, and red indicate Hemes #1 through #6 as labeled in Figure 2. Note that if the protonation of acid/base sites are coupled to the redox transitions, then the number of microstates shown for a given macrostate would increase by (*i.e.*, there would be two stacks of microstates for each acid/base site corresponding to when that site is protonated or deprotonated). The case shown is the simplest possible model.

It is computationally intractable to model by QM/MM@MD techniques the 64 microstates shown in Figure 3. For perspective, the computations by Guberman-Pfeffer[33] analyzed in Figures 2 and 4 involved 1.9 μs of production-stage molecular dynamics followed by $>3 \times 10^3$ QM/MM energy evaluations *just* to model the 7 microstates comprising the S0 and S1 macrostates (Figure 3). Fortunately, Portela *et al.*[24] found little difference between fitting six sequentially-coupled or six independent Nernst equations to the experimental titration curve.[40] This finding suggests that the potential at which each heme is reduced does not significantly depend on the redox state of any other heme. Transitions between macrostates are then equivalent to transitions between microstates in which only one heme is reduced (*i.e.*, only the six unique transitions from S0 to S1 in Figure 3 need to be considered). This independent-heme approximation, which is assessed below, has also been used in all modeling of redox conductivity in OmcS to date.[32-34] Thus, direct comparison between the six redox potentials from experiment and theory is possible.

A non-arbitrary way to compare the experimentally-derived and computationally-predicted redox potentials is to sort *both sets of potentials by the same rule* (*e.g.*, most negative to most positive potential). Doing so reveals (Figure 4 and Table S1 in the Supplementary Information) that the six independently predicted redox potentials by Guberman-Pfeffer,[33] starting from only the CryoEM structure, each come within chemical accuracy (≤0.05 eV) of an experimental redox potential. The maximum deviation between theory and experiment (<0.05 eV) is no greater than the standard deviation (0.05 eV) for each technique. It should be noted, however, that the six-parameter fit used by Portela *et al.* may suffer from the problem of von Neumann's elephant[41] (*i.e.*, there are too many adjustable parameters to give a unique solution). Portela *et al.* do not discuss performing a sensitivity analysis to see how the fit solution depends on the initial guess,

or how many different sets of six redox potentials can equivalently describe the titration curve in Figure 2.

Trusting at face-value the analysis of Portela *et al.*, however, the consistent agreement between experiment and theory empowers the modeling to serve as a 'rosette stone' to map the spectroelectrochemical potentials to specific hemes in the CryoEM structure (Figure 4).[42, 43] The sequence of hemes in order of increasingly positive (measured, computed) potential in volts versus SHE is: Heme #4 (-0.230±0.051, -0.248±0.036) < Heme #5 (-0.172±0.019, -0.177±0.024) < Heme #2 (-0.158±0.010, -0.111±0.027) < Heme #6 (-0.108±0.033, -0.095±0.031) < Heme #3 (-0.082±0.023, -0.071±0.027) < Heme #1 (-0.027±0.017, -0.063±0.034).

It is clear from Figure 4 that the linear sequence of hemes in the OmcS structure does not conform to the thermodynamic sequence of redox potentials. Electrons passing along the heme chain are geometrically constrained to changes in potential of 0.131, -0.076, 0.148, -0.058, -0.064, -0.081 V from Heme #1 of one subunit to Heme #1 in the next subunit. The implications of this potential 'roller-coaster' for electron transfer are discussed below. Structural determinants of the redox potentials, which are overwhelmingly electrostatic in origin, have already been delineated by Guberman-Pfeffer.[34]

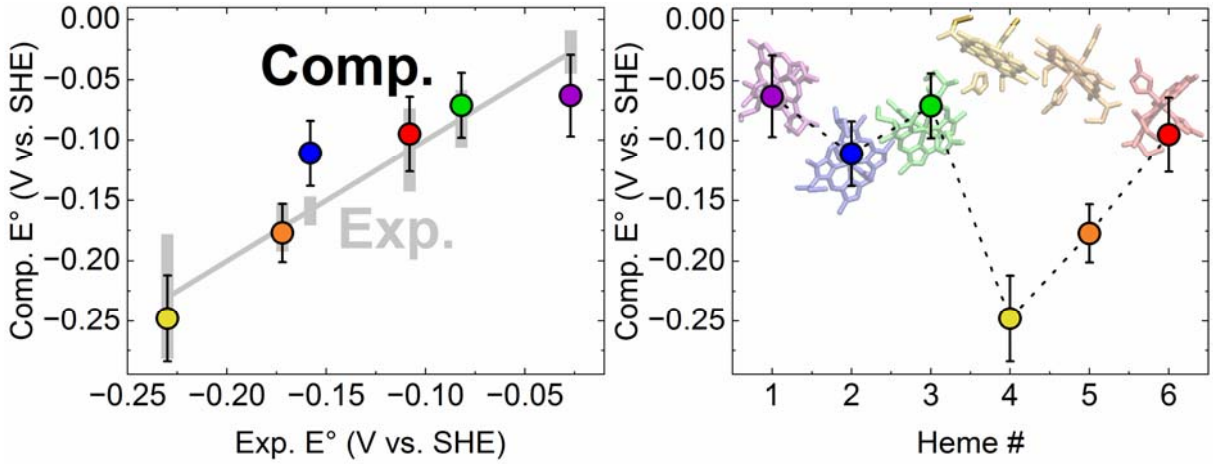

Figure 4. Redox potentials computed by Guberman-Pfeffer agree within 0.05 eV of the spectroelectrochemically measured potentials and define a potential 'roller-coaster' along the linear heme sequence in OmcS. Deviations from the diagonal in the computation (Comp.) versus experiment (Exp.) plot indicate differences from the experimental value. For the comparison to be non-arbitrary, the computed and measured redox potentials were both sorted in the same way before making a 1:1 mapping. The computed and experimental redox potentials are reproduced, respectively, from Portela *et al.*[24] and Guberman-Pfeffer.[33] The heme sequence comes from PDB 6EF8.[26] While visually interesting, no significance is ascribed to four of the redox potentials tracking (or the other two not tracking) the spatial arrangement of the hemes.

By contrast, the same experiment-versus-theory comparison (Table S1) reveals that two of the redox potentials predicted by Dahl *et al.* are 0.162 and 0.291 V too far negative, which explains the deviation between the solid blue and green curves at negative solution potentials in Figure 2. Because the discrepancy is not consistent for all the redox potentials predicted by Dahl *et al.*, the computed redox potential differences governing electron transfer between adjacent hemes were adversely affected in that work. Indeed, the unphysically negative potentials computed at 310 K created a large (∼|0.44| eV) free energy difference that was larger than any free energy difference computed at 270 K. The result was a severe underestimation of redox conductivity at 310 K, and the *apparent* agreement with experiment that conductivity is higher at the lower temperature (*anti*-Arrhenius kinetics); the right result for an experimentally disproven reason. Note that the discrepancy of the Dahl *et al.* work relative to spectroelectrochemistry performed in the same laboratory was known to the authors up to two years before publication,[44, 45] and some of the same authors on the Portela *et al.*[24] study do not comment on how the discrepancy invalidates their prior work.

Redox Cooperativities Dynamically fluctuate Potentials by ≤0.1 V under Electron Flux

As already noted, the computational predictions of Figures 2 and 4 approximated each redox transition as an independent event dominated by a single heme. In reality, however, each macroscopically observed redox transition by spectroelectrochemistry corresponds to a transition between ensembles of microstates in which different hemes are sequentially reduced (Figure 3). What is missing from the prior computations—and even experiments—for OmcS is a quantification of the redox cooperativities, or a measure of how much the redox potential of one heme is shifted by the oxidation of another heme. Portela *et al.* suggested redox cooperativities are comparable to the ≤0.05 V experimental uncertainties, which is consistent with the level of

agreement shown in Figure 4. But does an analysis of redox cooperativities using the CryoEM structure come to the same conclusion?

Redox cooperativities, often expressed as interaction energies, were recently predicted with quantitative accuracy for *de novo* designed solution-phase and membrane-embedded di-heme maquette proteins using the BioDC program.[46] BioDC[47] is an interactive Python workflow written by Guberman-Pfeffer that automates the computation of redox potentials, cooperativities, and conductivities in multi-heme cytochromes. As an additional benchmark, BioDC predicts interaction energies of 0.026 (Exp. 0.027±0.002)[48] eV between Hemes I and III and 0.026 (Exp. 0.041±0.003)[48] eV between Hemes III and IV (there is no Heme II) in the periplasmic *c*-type cytochrome isoform A (PpcA) from *G. sulfurreducens*. Given that the interaction energies are comparable to thermal energy at 300 K (0.03 eV) and only a single structure (not a thermal ensemble of structures) is considered for the calculations, the agreement is excellent.

Interestingly, application of the BioDC methodology to OmcS (Figure 5) indicates that *only* the oxidation of the first nearest neighbors along the spiral staircase of hemes shifts the redox potential of the heme on the adjacent rung by more than thermal energy at 300 K (~0.1 vs. 0.03 eV). This means that redox potentials dynamically fluctuate within 0.1 V in response to the flow of electrons through the filament. However, the comparison of fitting sequentially-coupled versus independent Nernst equations by Portela *et al.*, and the theory-experiment comparison assuming the latter model (Figures 2, 4) suggest that first-nearest neighbor cooperative interactions can be effectively neglected. This situation may be because the magnitude of the interactions is not much larger than the experimental or theoretical uncertainties in redox potentials (≤0.1 versus ≤0.05 V).

Heme #	1	2	3	4	5	6	1’
1	**-0.063**	0.085	0.025	0.015	0.007	0.005	0.004
2		**-0.111**	0.121	0.038	0.013	0.008	0.005
3			**-0.071**	0.095	0.025	0.015	0.007
4				**-0.248**	0.121	0.039	0.012
5					**-0.177**	0.068	0.018
6						**-0.095**	0.102
1’							**-0.063**

Figure 5. Heme-heme Interaction energy matrix expressed in upper-right triangle form. The diagonal elements (in V vs. SHE) are the redox potentials computed from quantum mechanics/molecular mechanics at molecular dynamics-generated configurations (QM/MM@MD). The off-diagonal elements (in eV) are interaction energies from Poisson-Boltzmann Surface Area calculations performed using the BioDC workflow. The prime mark (‘) indicates a heme that belongs to the next subunit in the filament.

Cooperativities of a similar (~0.08 eV) magnitude were previously reported from constant pH and redox molecular dynamics (C(E,pH)MD) simulations[33] by noting the difference in potentials when each heme was titrated with either all other hemes held in the fully oxidized state or allowed to be titrated. The ≤0.1 eV interaction energies in Figure 5 are also consistent with the prediction of a Debye-Hückel shielded electrostatics (DHSE) model[49] for heme groups separated by an Fe-to-Fe distance of ~8.2 Å, which is ~2 Å smaller on average than found in OmcS from either the CryoEM structure[25, 26] or hundreds of nanoseconds of classical molecular dynamics (Table S2 in the Supplementary Information).

The DHSE model was based on the analysis of redox cooperativities in 17 multiheme cytochromes from 5 different microbial genera,[48, 49] and assumed an effective dielectric constant (ϵ_{eff}) of 8.6. That the heme-heme interaction energy is larger than expected for the Fe-to-Fe separation found in OmcS suggests that the interactions are less effectively screened, or ϵ_{eff} is lower than assumed by the DHSE model. Indeed, the same modeling that accurately predicts the spectroelectrochemical potentials ascribed ϵ_{eff}s between 3 and 7 to the heme active sites in OmcS.

The analysis of redox cooperativities thus indicates that these interactions are (1) not much larger than thermal energy and experimental or computational uncertainties and can therefore be neglected and has (2) provided insight on the $\epsilon_{\mathrm{eff}}s$ of the heme binding sites. The first of these conclusions justifies the analysis of free energy landscapes for electron transfer based on the uncoupled heme redox potentials in the next section.

Structurally Assigned Spectroelectrochemical Potentials Define a Thermoneutral Free energy Landscape for Electron Transfer with ≤|0.18| eV Bumps

Figure 6 shows the experimental and computed reaction free energy (ΔG°, closed versus open green circles) landscapes based on the mapping in Figure 2 of spectroelectrochemical redox potentials to the CryoEM structure. Transport of an electron through a 'unit cell' of the filament is thermoneutral, even though ΔG° varies by as much as |0.18| eV along the heme chain. Thermoneutrality may be a 'design' strategy OmcS shares with the deca-heme metal-reducing cytochrome type F (MtrF) from *Shewanella oneidensis*.[50] In contrast to an evolutionary design principle proposed from the analysis of MtrF, however, the electronic coupling ($\langle H \rangle$, blue open diamonds in Figure 6) is greatest for the exergonic, instead of the endergonic steps.

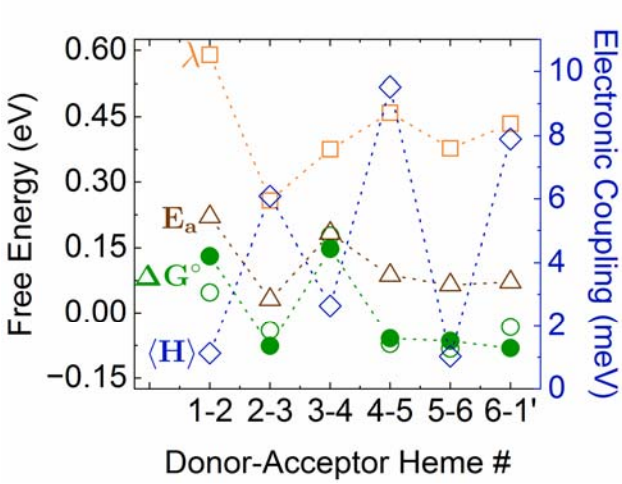

Figure 6. Reaction, reorganization, and activation free energies, as well as electronic couplings for heme-to-heme electron transfer through a 'unit cell' of the OmcS filament. The open and closed green circles represent the reaction free energy based on the computed redox potentials of Guberman-Pfeffer,[33] or the experimental spectroelectrochemical redox potentials from Portela *et al*.,[24] after assigning them to the CryoEM structure with the aid of the computations.

Reorganization Energies Empirically Accounting for Protein-Water Electronic Polarizability are 0.3 – 0.6 eV

Figure 6 also shows that ΔG° is not the only, or even the most important component of the activation energy (E_a, brown open triangles) for heme-to-heme electron transfer as defined by non-adiabatic Marcus theory:[51] $E_a = \frac{(\Delta G^\circ + \lambda)^2}{4\lambda}$. The reorganization energy (λ, orange open squares in Figure 6) has repeatedly been found in OmcS to be 0.5 – 1.0 eV from classical molecular dynamics simulations that neglect electronic polarizability,[30, 33, 34] as well as an approach based on the solvent accessibility of the heme group that was parameterized to reproduce λ from electronically polarizable molecular dynamics.[32]

Nonetheless, scaling factors of 0.56 – 0.80 have been recommended[52, 53] to correct λ computed from non-electronically polarizable simulations for the polarizability of the protein-water environment. To show the insensitivity of the following conclusions to the choice of this parameter (designated f_λ), both ends of the range will be used in the analysis. Figure 6 shows λ when $f_\lambda = 0.56$. Dynamical simulations performed with polarizable forcefields are needed to refine more precisely how much polarizability within OmcS reduces λ.

It has also been argued[54-56] that the change in electronic polarizability upon reduction of the heme cofactor in cytochrome *c* alone (*i.e.*, no correction for the polarizability of the environment)[55] is sufficient to bring simulations into accord with λ measured electrochemically. Using density functional theory (DFT) techniques that accurately reproduce the (iso/aniso)-tropic polarizabilities of rigid to semi-rigid molecules,[57-59] including a heme memetic,[60] the reduction-induced change in polarizability for His-Met (as in cytochrome *c*) and His-His (as in OmcS) ligated hemes is found both in vacuum and the protein-water environment to be much too small[61] (<15 Å^3 for iso- or anisotropic polarizability; see the *Assessment of Heme Electronic*

Polarizability section of the Supplementary information) to substantially change λ. Change in polarizability for the heme group upon reduction appears to be irrelevant for lowering electron transfer reorganization energy for hemoproteins in general.

The opposite finding reported previously[54] was premised on summing the contributions to the polarizability from vertical excitations computed within 10 eV of the ground state by the semi-empirical Zerner's Intermediate Neglect of Differential Overlap with Singles (ZINDO/S)[62, 63] approach. As the sum over excited states must grow to large (*e.g.*, 100)[54] numbers to converge the polarizability by this approach, increasingly larger errors accumulate when using a method parameterized to reproduce only the lowest-lying excited states. Furthermore, ZINDO/s, unlike DFT, has not been parameterized or benchmarked against experiment for computing polarizabilities.

This critique is in addition to the observation of Blumberger and co-workers[64, 65] that the result regarding the energetic influence of heme polarizability was extremely sensitive to small differences in the electric field variance experienced by the heme during molecular dynamics. which, in turn, has been shown to be overestimated by the non-polarizable forcefield used in those simulations.[66] There appear to be serious methodological reasons to consider with skepticism prior claims about heme polarizability lowering the reorganization energy for electron transfer.

Heme-to-Heme Electron Transfer Energetics are Conserved Among Cytochrome 'Nanowires'

The E_as for OmcS in Figure 6 are ≤0.22 eV. Similar E_as are predicted for all structurally characterized cytochrome 'nanowires' to date (Table S7 in the Supplementary Information). As with E_a, computations on OmcS[30, 32-34] and other multi-heme proteins with the same heme

packing motifs[50, 67] establish that $\langle H \rangle \leq 0.016$ eV. Thus, the two energetic quantities controlling the charge transfer rate (k_{et}) in the framework of non-adiabatic Marcus theory,

$$k_{ET} = \frac{2\pi\langle H^2 \rangle}{\hbar} \frac{e^{\frac{-E_a}{k_b T}}}{\sqrt{4\pi\lambda k_b T}} \quad (1),$$

are highly conserved. In eq 1, $\hbar$, k_b, and T are respectively the Plank constant, Boltzmann constant, and absolute temperature (300 K).

Pico- to Nanosecond Electron Transfers are Encoded by Heme Chains

Using the energetic quantities specific for OmcS (Figure 6), Eq. 1 returns electron transfer time constants $\left(\frac{1}{k_{ET}}\right)$ of (Table S8 in the Supplementary Information) 12 ps – 364 ns $(f_\lambda = 0.80)$ or 4 ps – 32 ns $(f_\lambda = 0.56)$. Similar time constants are expected for all other cytochrome 'nanowires' since the underlying energetics were shown above to be conserved. The time constants are not very sensitive to the assignment of spectroelectrochemical potentials to the specific hemes in the CryoEM structure. The range for $\frac{1}{k_{ET}}$ found by considering the $\Delta G°$s from all 6! or 720 ways of assigning the six potentials to the six hemes is 4 ps – 884 ns $(f_\lambda = 0.80)$ or 1 ps – 81 ns $(f_\lambda = 0.56)$. Thus, the conclusions of this analysis are robust and independent of the mapping of spectroelectrochemical potentials to specific hemes shown in Figure 4.

The average time constants for electron transfer between parallel- and perpendicularly-stacked heme pairs are found (Table S8 in the Supplementary Information) to be respectively 188 ps and 67 ns $(f_\lambda = 0.80)$, or 30 ps and 6 ns for $(f_\lambda = 0.56)$. These average time constants are in close agreement with the 360 ps and 11.9 ns average time constants experimentally determined by van Wonderen *et al.* from kinetic analyses of ultrafast transient absorption measurements on photosensitized variants of the metal reducing cytochrome type c (MtrC)[68] and the small tetraheme cytochrome,[69] both from *Shewanella oneidensis.*

General Energetic and Kinetic Constraints on Heme-to-Heme Electron transfer

The agreement across different multi-heme proteins from distinct organisms is a natural consequence of the following considerations for the three energetic parameters ($\langle H \rangle$, ΔG°, and λ) that govern non-adiabatic Marcus theory rates:

(1) The $\langle H \rangle$ is principally determined by the distance and orientation of the charge donating and accepting heme groups.[70, 71] These geometrical descriptors for heme packing motifs are highly conserved.[4] For the two most common packing motifs, the $\langle H \rangle$ has been computed to be ≤0.016 eV regardless of the employed computational approach.[30, 32, 34, 67, 72]

(2) The minimum edge-to-edge van der Waals distance between adjacent hemes in the conserved packing motifs ensures both hemes experience a similar electrostatic environment. Because the electrostatic environment overwhelmingly tunes heme redox potentials (as opposed to conformational distortions of the semi-rigid cofactor),[34] adjacent hemes that are chemically identical (same peripheral substituents and axial ligands) will have similar redox potentials, or a small redox potential difference (*i.e.*, a small ΔG° for electron transfer). For several multi-heme cytochromes studied to date, ΔG° is ≤|0.3| eV.[32, 34, 47, 67, 72]

(3) Reorganization energy due to changes in the internal coordinates of the heme group upon reduction/oxidation are intrinsic to the cofactor and contribute ~0.1 eV to E_a.[73, 74] Reorganization energy from the protein-water matrix is a collective property of the environment, with as much as 50% coming from the solvent.[75] Binding sites with similar dielectric properties may be expected to bind the same cofactor, and thus, to have similar reorganization energies. In general, λ is expected from experimental work to be 0.8 eV,[76] consistent with what has been found computationally (0.7 – 1.1 eV) for heme proteins.[32, 34, 47, 64, 67, 72, 75]

Two mechanisms are known to lower λ, namely an incomplete sampling of environment relaxation modes coupled to charge transfer on the timescale of the reaction (called non-ergodicity) and active site polarizability. Microseconds of molecular dynamics on cytochrome 'nanowires',[30, 33, 34] and extensive simulations on cytochrome *c*,[64] have not yet given any indication that ergodicity-breaking is relevant for heme systems. A large change in polarizability upon reduction has been computationally claimed for the heme cofactor of cytochrome *c*, but as discussed above, that assertion does not withstand the test of more rigorous and validated computations (Tables S3-S6). Ultimately, the extent to which the polarizability of the heme group changes upon reduction needs to be assessed experimentally to conclusively resolve this matter. When comparing theory and experiment, however, it is critical to ensure that the conditions for determining λ are comparable: Experimental measures of λ for cytochrome *c* alone range from 0.2 – 1.1 eV[77, 78] depending on whether or not the protein is adsorbed to a self-assembled monolayer (SAM)-coated electrode, and if so, the nature of the protein-SAM interface.

Taken together, these considerations suggest that strongly conserved heme packing geometries and active sites of a similar dielectric profile for binding the same heme cofactor impose energetic constraints ($\langle \mathrm{H} \rangle \leq 0.016$ eV, $\Delta \mathrm{G}^{\circ} \leq |0.3|\, eV$, and $\lambda \geq 0.5$ eV), and therefore kinetic constrains (ps – ns) that are expected to apply to all biological heme-to-heme electron transfer reactions. In this view,[34] cytochrome filaments comprise a functionally robust heme chain whose operation is largely insensitive to variations in the surrounding protein 'insulation' that has been tailored by evolution to form a habitat-customized interface for exchanging electrons with minerals, metals, or other microbes. The question, however, is: Can this universal picture of

protein electron transfer reasonably account for the exodus of >10^5 electrons/s/cell (>fA/cell) from an electrogenic microorganism (electrogen) like *G. sulfurreducens*?

≥5 Filaments/cell Observed Experimentally are Predicted to suffice for Cellular Respiration

The set of k_{ET}s for moving an electron through a 'unit cell' of the OmcS filament (Table S8 in the Supplementary Information) can be used to evaluate the analytical Derrida formula[79] for diffusive charge hopping along the periodic (pseudo)-one-dimensional heme chain of the cytochrome homopolymer. Doing so delivers a diffusion constant that is 1.4×10^{-2} $(f_\lambda = 0.80)$ or 1.3×10^{-1} $(f_\lambda = 0.56)$ nm^2/ns, which should be compared to the diffusion constant of ~0.6 nm^2/ns required by cellular respiration (see the Derivation of a *Diffusion Constant from the Cellular Respiratory Rate* section in the Supplementary Information). The comparison suggests that between 44 $(f_\lambda = 0.80)$ to 5 $(f_\lambda = 0.56)$ filaments/cell are needed, and it is known that *G. sulfurreducens* expresses ≥20 filaments/cell. A previous estimate of ~7 filaments/cell was found for a generic heme chain using the average of experimental time constants for electron transfer within perpendicular- and parallel-displaced stacked heme pairs.[22] The implications are that either f_λ of 0.56 or 0.80 is consistent with experiment, and more importantly, ≥5 OmcS 'nanowires' are sufficient for cellular respiration via extracellular electron transfer.

Note that comparisons with diffusion constants of 8 – 3700 nm^2/ns implied by conductivities measured with AFM (see the *Derivation of Diffusion Constants from Experimentally Measured Conductivities* section in the Supplementary Information) are not warranted because, as discussed elsewhere,[22] those experiments suffer from artifacts of the measurement conditions (*e.g.*, adsorption on bear substrates, dehydration, and compression), and may probe structures that deviate from the CryoEM models, or abiological charge transport (instead of transfer)[80]

Given that the cellular respiratory flux can be discharged by a physiologically meaningful number of filaments in the limit of a redox relay model, but the same model underestimates the AFM-measured conductivity by >60-fold, supports the view that some abiological mechanism is operative in the latter case.

Conclusion

To summarize, a non-arbitrary comparison finds heme redox potentials computed from the CryoEM structure of OmcS and those reported 15-months later by spectroelectrochemistry to all agree within chemical accuracy (<0.05 eV). The consistent theory-experiment agreement enables an unambiguous assignment of the spectroelectrochemical redox potentials to specific hemes in the CryoEM structure, which is not presently possible by experimental methods. The potentials are predicted to dynamically shift by ≤0.1 V due to redox cooperativities between the hemes, an effect that could also not be resolved experimentally, but is consistent with prior literature.

The structurally-assigned redox potentials define a bumpy but overall thermoneutral free energy landscape for electrons that pass through a 'unit cell' of the homopolymer. When paired in the framework of non-adiabatic Marcus theory with computed electronic couplings and reorganization energies empirically corrected for protein-water electronic polarizability, pico- to nanosecond heme-to-heme electron transfer rates are obtained that agree with computational and experimental kinetic analyses of other multi-heme systems that show the same heme packing geometries. These rates specify a diffusion constant that implies ≥5 filaments are needed to discharge the metabolic electrons of a *G. sulfurreducens* cell, which is consistent with the number of filaments/cell observed experimentally.

The van der Waals packing of heme pairs in highly conserved geometries within binding sites that likely have a similar dielectric profile for accommodating the same redox cofactor imposes

universal energetic and kinetic constraints on electron transfer through multi-heme cytochromes. This conclusion is supported by an analysis of all structurally characterized cytochrome 'nanowires' to date. Thus, a universal picture applicable to multi-heme chains in all kingdoms of life emerges from the foregoing computational analysis that connects cryogenic electron microscopy, spectroelectrochemistry, and cellular respiration.

Methods

Simulation of Spectroelectrochemical Titration Curve

For a system like OmcS with non- to weakly interacting redox centers, the fraction of reduced species as a function of the solution potential (*i.e.*, the spectroelectrochemical titration curve) can be approximated by a sum of independent Nernst equations,

$$f_{red} \approx \sum_{i=1}^{m} \frac{1}{1 + e^{\frac{n\nu(E - E_i^\circ)}{k_b T}}} \tag{1}$$

where f_{red}, m, n, ν, E_i°, E, k_b, and T respectively signify the total reduced fraction, the number of redox-active centers (6 for OmcS), the Hill coefficient describing redox cooperativities in a *post hoc* fashion (assumed to be unity), the number of transferred electrons (each heme is a one-electron acceptor), the redox potential of the ith heme (taken from either Dahl *et al.*[30] or Guberman-Pfeffer[33]), the solution potential (±2 V), the Boltzmann constant, and absolute temperature (300 K). A Python program implementing Eq. 1 (CompareExpAndCalcRedoxTitrationAnalysis.py) was written to generate the data shown in Figure 2 and is available at the Zenodo repository accompanying this manuscript.[81]

Computation of Redox Potentials

The QM/MM@MD methodology was extensively described in section S1.3.2 of the Supporting Information to Ref. 33; a brief description follows here for context. The six redox

potentials compared in the present work to spectroelectrochemistry were presented in Table S11 of Ref. 33

The redox potential of each heme was computed as

$$E^{\circ} = \frac{\Delta G^{\circ}_{ox}}{nF} + E_{ref} \quad (2)$$

where $n = 1$ for the number of electrons accepted by each heme; F is the Faraday constant, and $E_{ref} = 4.32$ V to put the computed redox potentials on the same Standard Hydrogen Electrode (SHE) scale as the spectroelectrochemical potentials reported by Portela *et al.*[24] The value used for E_{ref} is the absolute potential of SHE corrected for the integrated heat capacity and entropy of the electron.[82] Very importantly, $E_{ref} = 4.32$ V was used for *all* computed redox potentials, meaning that the consistent level of agreement with experiment across the set of potentials, and the differences in computed redox potentials that govern electron transfer are independent of the particular value chosen for E_{ref}.

ΔG°_{ox} was computed by Eq. 3 under the approximation that the polarization of the environment (and therefore the free energy of 'solvation') is a linear function of the charge on the solute (*i.e.*, the linear response approximation, LRA).

$$\Delta G_{ox} = \frac{1}{2}\left(\langle E_{VertIP}\rangle_{red} + \langle E_{-VertEA}\rangle_{ox}\right) \quad (3)$$

In Eq. 3, $\langle E_{VertIP}\rangle_{red}$ is the vertical ionization potential thermally averaged over configurations with the given heme in the reduced state, whereas $\langle E_{-VertEA}\rangle_{ox}$ is the negative of the vertical electron affinity computed over thermally averaged configurations with the given heme in the oxidized state. The vertical energy in either ensemble is given by the difference in energy between the oxidized and reduced electronic states at the same nuclear geometry, $E_{ox}(r_x) - E_{red}(r_x)$, where x specifies the oxidized or reduced ensemble for the heme being considered in

two oxidation states. Note that the free energy contribution from bulk solvation[82] was omitted because it was found[33] to be similar to thermal energy at 300 K.

To evaluate $\langle \mathrm{E_{VertIP}} \rangle_{\mathrm{red}}$ and $\langle \mathrm{E_{-VertEA}} \rangle_{\mathrm{ox}}$, classical molecular dynamics simulations was previously performed[33] in which either all hemes were oxidized, or one heme was reduced while all other hemes remained oxidized. The all-heme-oxidized trajectory was propagated for 252 ns, whereas the single-heme-reduced trajectories were propagated for 301, 281, 266, 295, 242, and 294 ns, respectively, for Hemes #1 through #6. The AMBER FF99SB forcefield[83] was used for the protein, whereas parameters for the heme cofactor were adopted from Crespo *et a*.[84] and Henriques *et al.*,[85] The TIP3P water model[86] and the monovalent ion parameters of Joung and Cheatham[87] were used to model the solution state.

With 1.9 μs of simulations in hand, configurations for each of the six hemes in the fully oxidized ensemble, and the reduced heme in each of the single-heme-reduced-ensembles were sampled and submitted to electronically-embedded QM/MM energy evaluations for the given heme in both the reduced and oxidized electronic states at the same nuclear geometry (*i.e.*, two QM/MM single point calculations for each sampled configuration for each heme). The number of configurations sampled in the (all-heme-oxidized, single-heme-reduced) ensembles for each heme were: Heme #1 (100, 107); Heme #2 (154, 150); Heme #3 (131, 130); Heme #4 (128, 120); Heme #5 (139, 168); Heme #6 (112, 87). A total of $(1526\ \mathrm{frames}) \times (2\ \mathrm{single-point\ calculations/frame}) = 3052\ \mathrm{calculations}$ were performed on a 93-atom QM region (*i.e.*, the cofactor shown in Figure 1 but with hydrogens present), embedded in the electrostatic environment of the protein-water matrix, using the B3LYP approximate density functional[88-90] and a mixed, triple-ζ basis set: The LANL2TZ[91, 92]

effective core potential and valance basis sets for Fe, and the 6-311G(d) basis set[93-95] for H, C, N and S atoms. All QM calculations were performed with Gaussian 16 Rev. A.03.[96]

The distributions for both $\langle E_{VertIP} \rangle_{red}$ and $\langle E_{-VertEA} \rangle_{ox}$ calculated in this way were found to be symmetric, Gaussian-shaped, and of equal width, which are the conditions required for the LRA approximation to apply.

Computation of Reorganization Energies and Electronic Couplings

The methods and data for these quantities were previously published in Ref. 33.

Computation of Redox Cooperativities

The BioDC Python workflow[47] for computation of redox potentials, cooperativities, and conductivities was used for the second of these purposes here. The program, as well as all files related to this particular example case are available at the Zenodo repository accompanying this manuscript.[81]

Experimental reports of redox cooperativities typically take the state in which all redox centers are reduced as the reference.[40] The same all-heme-reduced state was taken as the reference for the redox cooperativity calculations. From this reference state, the difference in oxidation energy for heme i when heme j is oxidized versus reduced was computed for all possible pairings of hemes where $i \neq j$. The resulting energy is how much the oxidation of heme i is disfavored by the oxidation of heme j.

BioDC provides an interface for computing the energies with the Poisson-Boltzmann Surface Area model of the AmberTools package in which the protein is immersed in an implicit aqueous solvent.[97] To that end, BioDC estimates the static dielectric constant based on the solvent accessibility[32] of every adjacent heme pair and takes the average of these values as the static dielectric constant for all possible pairings of hemes in the redox cooperativity calculations.

Computation of Heme Electronic Polarizability

The change in electronic polarizability between reduced and oxidized electronic states was computed (1) in vacuum for models of His-His and His-Met-ligated *c*-type hemes; (2) configurations of the His-Met-ligated *c*-type heme of cytochrome *c* sampled in the protein-water matrix during molecular dynamics; and (3) configurations for each of the six His-His-ligated c-type hemes of OmcS sampled in the protein-water matrix during molecular dynamics.

Model hemes in Vacuum calculations. Deachapunya *et al.*[60] showed that the electronic polarizability of tetraphenylporphyrin-ironIII chloride (FeTPPCl) can be quantitatively reproduced (Calc. 113.4 $Å^3$ versus Exp. 102±11 $Å^3$) by optimizing the geometry in vacuum with the BLYP functional and the 6-31G(d) basis set, followed by a polarizability calculation with the same functional but with polarization functions added to the basis set (6-31+G(d)). Therefore, the models of His-His- and His-Met-ligated *c*-type heme cofactors shown in Figure S1 of the Supplementary Information were optimized with the BLYP/6-31G(d) model chemistry. Each of the heme models were optimized in the reduced and oxidized electronic states. Harmonic frequency analyses confirmed that a local minimum on the ground state potential energy surface had been found in every case (*i.e.*, no negative frequencies). The atomic coordinates of the optimized geometries are provided in CoordinatesForModelHemeSystem.xlsx.

Subsequent calculation of the electronic polarizability was performed with a variety of approximate functionals and basis set combinations, as shown in Table S7.

His-Met-Ligated c-type Heme of Cytochrome c. The polarizability calculations for a His-Met-ligated heme were repeated, but now at geometries sampled during classical molecular dynamics within the cytochrome *c* active site. Separate molecular dynamics trajectories were performed with the charge distribution on the heme corresponding to the reduced and oxidized states. From

each of these ensembles, 200 snapshots were selected randomly so long as the minimum time increment between the snapshots was >20 ps. The polarizability was computed for the heme at each configuration in the oxidized electronic state with and without the protein-water environment, as well as in the reduced electronic state with and without the protein-water environment. The results are summarized in Table S4 and S5 of the Supplementary Information; the polarizability tensor computed at each frame is provided in PerFramePolarizabilities.xlsx. The polarizability calculations were performed with the BLYP functional, the LANL2DZ effective core and valance basis sets for Fe, and the 6-31G(d) basis set for H, C, N, and S atoms.

His-His-Ligated c-type Hemes of OmcS. A set of 250 snapshots were randomly selected with a minimum time increment of >20 ps from molecular dynamics trajectories in which each of the six hemes were in the reduced state. At each frame, the electronic polarizability was computed in the oxidized and reduced electronic states. The polarizability was computed with the BLYP/6-31G(d) model chemistry. The results are summarized in Table S4 and S6 of the Supplementary Information; the polarizability tensor computed at each frame is provided in PerFramePolarizabilities.xlsx.

Data Availability

Data relevant to the main conclusions are provided in the PDF and XLSX Supplementary files, and the Zenodo repository accompanying this manuscript (https://doi.org/10.5281/zenodo.10906110). Any other data is available upon request.

Code Availability

All custom programs developed for this study are available in an accompanying Zenodo repository that is publicly accessible at https://doi.org/10.5281/zenodo.10906110.

Author Contributions

All aspects of this study including conceptualization, exclusion, analysis, and manuscript writing were performed by M. J. G-P.

Competing Interests

There are no competing interests to disclose.

Materials and Correspondence

All correspondence and material requests should be directed to M. J. G-P at Matthe_Guberman-Pfe@Baylor.edu.

References

(1) Jiang, X.; Hu, J.; Petersen, E. R.; Fitzgerald, L. A.; Jackan, C. S.; Lieber, A. M.; Ringeisen, B. R.; Lieber, C. M.; Biffinger, J. C. Probing single-to multi-cell level charge transport in Geobacter sulfurreducens DL-1. *Nat. Comm.* **2013**, *4* (1), 2751.

(2) Karamash, M.; Stumpe, M.; Dengjel, J.; Salgueiro, C. A.; Giese, B.; Fromm, K. M. Reduction Kinetic of Water Soluble Metal Salts by Geobacter sulfurreducens: Fe2+/Hemes Stabilize and Regulate Electron Flux Rates. *Front. Microbiol.* **2022**, *13*, 909109.

(3) Lampa-Pastirk, S.; Veazey, J. P.; Walsh, K. A.; Feliciano, G. T.; Steidl, R. J.; Tessmer, S. H.; Reguera, G. Thermally activated charge transport in microbial protein nanowires. *Sci. Rep.* **2016**, *6* (1), 23517.

(4) Baquero, D. P.; Cvirkaite-Krupovic, V.; Hu, S. S.; Fields, J. L.; Liu, X.; Rensing, C.; Egelman, E. H.; Krupovic, M.; Wang, F. Extracellular cytochrome nanowires appear to be ubiquitous in prokaryotes. In *Cell*, 2023; Vol. 186, pp 1-12.

(5) Lovley, D. R. Syntrophy goes electric: direct interspecies electron transfer. *Annu. Rev. Microbiol.* **2017**, *71*, 643-664.

(6) Nealson, K. H.; Saffarini, D. Iron and manganese in anaerobic respiration: environmental significance, physiology, and regulation. *Annu. Rev. Microbiol.* **1994**, *48* (1), 311-343.

(7) Vargas, M.; Kashefi, K.; Blunt-Harris, E. L.; Lovley, D. R. Microbiological evidence for Fe (III) reduction on early Earth. *Nature* **1998**, *395* (6697), 65-67.

(8) Lovley, D. R.; Holmes, D. E. Electromicrobiology: the ecophysiology of phylogenetically diverse electroactive microorganisms. *Nat. Rev. Microbiol.* **2022**, *20* (1), 5-19.

(9) Zhao, J.; Li, F.; Cao, Y.; Zhang, X.; Chen, T.; Song, H.; Wang, Z. Microbial extracellular electron transfer and strategies for engineering electroactive microorganisms. *Biotechnol. Adv.* **2021**, *53*, 107682.

(10) Jiang, Y.; Shi, M.; Shi, L. Molecular underpinnings for microbial extracellular electron transfer during biogeochemical cycling of earth elements. *Sci. China Life Sci.* **2019**, *62*, 1275-1286.

(11) Zhang, X.; Yuan, Z.; Hu, S. Anaerobic oxidation of methane mediated by microbial extracellular respiration. *Environ. Microbiol. Rep.* **2021**, *13* (6), 790-804.

(12) Gu, T.; Wang, D.; Lekbach, Y.; Xu, D. Extracellular electron transfer in microbial biocorrosion. *Curr. Opin. Electrochem.* **2021**, *29*, 100763.

(13) Jelen, B. I.; Giovannelli, D.; Falkowski, P. G. The role of microbial electron transfer in the coevolution of the biosphere and geosphere. *Annu. Rev. Microbiol.* **2016**, *70*, 45-62.

(14) Lovley, D. R.; Yao, J. Intrinsically conductive microbial nanowires for ‘green’electronics with novel functions. *Trends Biotechnol.* **2021**, *39* (9), 940-952.

(15) Sun, Y. L.; Tang, H. Y.; Ribbe, A.; Duzhko, V.; Woodard, T. L.; Ward, J. E.; Bai, Y.; Nevin, K. P.; Nonnenmann, S. S.; Russell, T. Conductive composite materials fabricated from microbially produced protein nanowires. *Small* **2018**, *14* (44), 1802624.

(16) Lovley, D. R. e-Biologics: fabrication of sustainable electronics with “green” biological materials. *MBio* **2017**, *8* (3), 10.1128/mbio. 00695-00617.

(17) Zou, L.; Zhu, F.; Long, Z.-e.; Huang, Y. Bacterial extracellular electron transfer: a powerful route to the green biosynthesis of inorganic nanomaterials for multifunctional applications. *J. Nanobiotechnol.* **2021**, *19* (1), 120.

(18) Malvankar, N. S.; Lovley, D. R. Microbial nanowires for bioenergy applications. *Curr. Opin. Biotechnol.* **2014**, *27*, 88-95. DOI: 10.1016/j.copbio.2013.12.003 From NLM Medline.

(19) Zhang, Y.; Hsu, L. H.-H.; Jiang, X. Living electronics. *Nano Res.* **2020**, *13*, 1205-1213.

(20) Sanjuan-Alberte, P.; Alexander, M. R.; Hague, R. J.; Rawson, F. J. Electrochemically stimulating developments in bioelectronic medicine. *Bioelectron. Med.* **2018**, *4*, 1-7.

(21) Bird, L. J.; Kundu, B. B.; Tschirhart, T.; Corts, A. D.; Su, L.; Gralnick, J. A.; Ajo-Franklin, C. M.; Glaven, S. M. Engineering wired life: synthetic biology for electroactive bacteria. *ACS Synth. Biol.* **2021**, *10* (11), 2808-2823.

(22) Guberman-Pfeffer, M. J. To be or Not to be a Cytochrome: Electrical Characterizations are Inconsistent with Geobacter Cytochrome'Nanowires'. *Front. Microbiol.* **2024**, *15*, 1397124.

(23) Silva, M. A.; Fernandes, A. P.; Turner, D. L.; Salgueiro, C. A. A biochemical deconstruction-based strategy to assist the characterization of bacterial electric conductive filaments. *Int. J. Mol. Sci.* **2023**, *24* (8), 7032.

(24) Portela, P. C.; Shipps, C. C.; Shen, C.; Srikanth, V.; Salgueiro, C. A.; Malvankar, N. S. Widespread extracellular electron transfer pathways for charging microbial cytochrome OmcS nanowires via periplasmic cytochromes PpcABCDE. *Nat. Comm.* **2024**, *15* (1), 2434. DOI: 10.1038/s41467-024-46192-0.

(25) Filman, D. J.; Marino, S. F.; Ward, J. E.; Yang, L.; Mester, Z.; Bullitt, E.; Lovley, D. R.; Strauss, M. Cryo-EM reveals the structural basis of long-range electron transport in a cytochrome-based bacterial nanowire. *Commun. Biol.* **2019**, *2* (1), 219.

(26) Wang, F.; Gu, Y.; O'Brien, J. P.; Sophia, M. Y.; Yalcin, S. E.; Srikanth, V.; Shen, C.; Vu, D.; Ing, N. L.; Hochbaum, A. I. Structure of microbial nanowires reveals stacked hemes that transport electrons over micrometers. *Cell* **2019**, *177* (2), 361-369. e310.

(27) Wang, F.; Mustafa, K.; Suciu, V.; Joshi, K.; Chan, C. H.; Choi, S.; Su, Z.; Si, D.; Hochbaum, A. I.; Egelman, E. H. Cryo-EM structure of an extracellular Geobacter OmcE cytochrome filament reveals tetrahaem packing. *Nat. Microbiol.* **2022**, *7* (8), 1291-1300.

(28) Gu, Y.; Guberman-Pfeffer, M. J.; Srikanth, V.; Shen, C.; Giska, F.; Gupta, K.; Londer, Y.; Samatey, F. A.; Batista, V. S.; Malvankar, N. S. Structure of Geobacter cytochrome OmcZ identifies mechanism of nanowire assembly and conductivity. *Nat. Microbiol.* **2023**, *8* (2), 284-298.

(29) Humphrey, W.; Dalke, A.; Schulten, K. VMD: visual molecular dynamics. *J. Mol. Graph.* **1996**, *14* (1), 33-38.

(30) Dahl, P. J.; Yi, S. M.; Gu, Y.; Acharya, A.; Shipps, C.; Neu, J.; O'Brien, J. P.; Morzan, U. N.; Chaudhuri, S.; Guberman-Pfeffer, M. J. A 300-fold conductivity increase in microbial cytochrome nanowires due to temperature-induced restructuring of hydrogen bonding networks. *Sci. Adv.* **2022**, *8* (19), eabm7193.

(31) Eshel, Y.; Peskin, U.; Amdursky, N. Coherence-assisted electron diffusion across the multi-heme protein-based bacterial nanowire. *Nanotechnology* **2020**, *31* (31), 314002.

(32) Jiang, X.; van Wonderen, J. H.; Butt, J. N.; Edwards, M. J.; Clarke, T. A.; Blumberger, J. Which Multi-Heme Protein Complex Transfers Electrons More Efficiently? Comparing MtrCAB

from Shewanella with OmcS from Geobacter. *J. Phys. Chem. Lett.* **2020**, *11* (21), 9421-9425. DOI: 10.1021/acs.jpclett.0c02842 From NLM Medline.

(33) Guberman-Pfeffer, M. J. Assessing Thermal Response of Redox Conduction for Anti-Arrhenius Kinetics in a Microbial Cytochrome Nanowire. *J. Phys. Chem. B* **2022**, *126* (48), 10083-10097. DOI: 10.1021/acs.jpcb.2c06822 From NLM Medline.

(34) Guberman-Pfeffer, M. J. Structural Determinants of Redox Conduction Favor Robustness over Tunability in Microbial Cytochrome Nanowires. *J. Phys. Chem. B* **2023**, *127* (32), 7148-7161. DOI: 10.1021/acs.jpcb.3c02912 From NLM Medline.

(35) Livernois, W.; Anantram, M. Quantum transport in conductive bacterial nanowires. In *2021 IEEE 16th Nanotechnology Materials and Devices Conference (NMDC)*, 2021; IEEE: pp 1-5.

(36) Livernois, W.; Anantram, M. P. A Spin-Dependent Model for Multi-Heme Bacterial Nanowires. *ACS Nano.* **2023**, *17* (10), 9059-9068. DOI: 10.1021/acsnano.2c12027 From NLM Medline.

(37) Yalcin, S. E.; O'Brien, J. P.; Gu, Y.; Reiss, K.; Yi, S. M.; Jain, R.; Srikanth, V.; Dahl, P. J.; Huynh, W.; Vu, D. Electric field stimulates production of highly conductive microbial OmcZ nanowires. *Nat. Chem. Bio.* **2020**, *16* (10), 1136-1142.

(38) Tan, Y.; Adhikari, R. Y.; Malvankar, N. S.; Ward, J. E.; Nevin, K. P.; Woodard, T. L.; Smith, J. A.; Snoeyenbos-West, O. L.; Franks, A. E.; Tuominen, M. T. The low conductivity of Geobacter uraniireducens pili suggests a diversity of extracellular electron transfer mechanisms in the genus Geobacter. *Front. Microbiol.* **2016**, *7*, 980.

(39) Strycharz-Glaven, S. M.; Snider, R. M.; Guiseppi-Elie, A.; Tender, L. M. On the electrical conductivity of microbial nanowires and biofilms. *Energy Environ. Sci.* **2011**, *4* (11). DOI: 10.1039/c1ee01753e.

(40) Paquete, C. M.; Louro, R. O. Unveiling the details of electron transfer in multicenter redox proteins. *Acc. Chem. Res.* **2014**, *47* (1), 56-65.

(41) Dyson, F. A meeting with Enrico Fermi. *Nature* **2004**, *427* (6972), 297-297.

(42) Daidone, I.; Paltrinieri, L.; Amadei, A.; Battistuzzi, G.; Sola, M.; Borsari, M.; Bortolotti, C. A. Unambiguous assignment of reduction potentials in diheme cytochromes. *J. Phys. Chem. B* **2014**, *118* (27), 7554-7560.

(43) Cruzeiro, V. W. D.; Feliciano, G. T.; Roitberg, A. E. Exploring coupled redox and pH processes with a force-field-based approach: applications to five different systems. *J. Am. Chem. Soc.* **2020**, *142* (8), 3823-3835.

(44) OBrien, J. P. A Tale of Two Nanowires: the Biochemical and Spectroscopic Characterization of the Conductive Cytochrome OmcS and OmcZ Filaments of Geobacter Sulfurreducens. Yale University, 2020.

(45) Shipps, C. Electrons on the Move in Proteins: Microbial Cytochrome Nanowires in Extracellular Electron Transfer and as Functional Materials. Ph.D., Yale University, United States -- Connecticut, 2022.

(46) Hardy, B. J.; Dubiel, P.; Bungay, E. L.; Rudin, M.; Williams, C.; Arthur, C. J.; Guberman-Pfeffer, M. J.; Oliveira, A. S. F.; Curnow, P.; Anderson, J. R. Delineating redox cooperativity in water-soluble and membrane multiheme cytochromes through protein design. *bioRxiv* **2024**, 2024.2003. 2021.586059.

(47) Guberman-Pfeffer, M. J. From Hot Water to Dry Dirt: Microbes Use Cytochrome'Nanowires' of Similar Conductivity but Different Structure. *bioRxiv* **2023**, 2023.2006. 2012.544705.

(48) Morgado, L.; Bruix, M.; Pessanha, M.; Londer, Y. Y.; Salgueiro, C. A. Thermodynamic characterization of a triheme cytochrome family from Geobacter sulfurreducens reveals mechanistic and functional diversity. *Biophys. J.* **2010**, *99* (1), 293-301.

(49) Fonseca, B. M.; Paquete, C. M.; Salgueiro, C. A.; Louro, R. O. The role of intramolecular interactions in the functional control of multiheme cytochromes c. *FEBS Lett.* **2012**, *586* (5), 504-509.

(50) Breuer, M.; Rosso, K. M.; Blumberger, J. Electron flow in multiheme bacterial cytochromes is a balancing act between heme electronic interaction and redox potentials. *Proc. Natl. Acad. Sci. U. S. A.* **2014**, *111* (2), 611-616. DOI: 10.1073/pnas.1316156111 From NLM Medline.

(51) Marcus, R. A.; Sutin, N. Electron transfers in chemistry and biology. *Biochim. Biophys. Acta, Rev. Bioenerg.* **1985**, *811* (3), 265-322.

(52) Kontkanen, O. V.; Biriukov, D.; Futera, Z. Reorganization free energy of copper proteins in solution, in vacuum, and on metal surfaces. *J. Chem. Phys.* **2022**, *156* (17).

(53) Matyushov, D. V. Reorganization energy of electron transfer. *Phys. Chem. Chem. Phys.* **2023**, *25* (11), 7589-7610.

(54) Dinpajooh, M.; Martin, D. R.; Matyushov, D. V. Polarizability of the active site of cytochrome c reduces the activation barrier for electron transfer. *Sci. Rep.* **2016**, *6* (1), 28152.

(55) Seyedi, S. S.; Waskasi, M. M.; Matyushov, D. V. Theory and electrochemistry of cytochrome c. *J. Phys. Chem. B* **2017**, *121* (19), 4958-4967.

(56) Martin, D. R.; Dinpajooh, M.; Matyushov, D. V. Polarizability of the active site in enzymatic catalysis: Cytochrome c. *J. Phys. Chem. B* **2019**, *123* (50), 10691-10699.

(57) Hickey, A. L.; Rowley, C. N. Benchmarking quantum chemical methods for the calculation of molecular dipole moments and polarizabilities. *J. Phys. Chem. A* **2014**, *118* (20), 3678-3687.

(58) Pabst, F.; Blochowicz, T. On the intensity of light scattered by molecular liquids—Comparison of experiment and quantum chemical calculations. *J. Chem. Phys.* **2022**, *157* (24).

(59) Hait, D.; Head-Gordon, M. How accurate are static polarizability predictions from density functional theory? An assessment over 132 species at equilibrium geometry. *Phys. Chem. Chem. Phys.* **2018**, *20* (30), 19800-19810.

(60) Deachapunya, S.; Stefanov, A.; Berninger, M.; Ulbricht, H.; Reiger, E.; Doltsinis, N. L.; Arndt, M. Thermal and electrical properties of porphyrin derivatives and their relevance for molecule interferometry. *J. Chem. Phys.* **2007**, *126* (16).

(61) Sarhangi, S. M.; Matyushov, D. V. Comment on "Applicability of perturbed matrix method for charge transfer studies at bio/metallic interfaces: a case of azurin" by O. Kontkanen, D. Biriukov and Z. Futera, Phys. Chem. Chem. Phys., 2023, 25, 12479. *Phys. Chem. Chem. Phys.* **2023**, *25* (39), 26923-26928.

(62) Zerner, M. C.; Loew, G. H.; Kirchner, R. F.; Mueller-Westerhoff, U. T. An intermediate neglect of differential overlap technique for spectroscopy of transition-metal complexes. Ferrocene. *J. Am. Chem. Soc.* **1980**, *102* (2), 589-599.

(63) Hanson, L. K.; Fajer, J.; Thompson, M. A.; Zerner, M. C. Electrochromic effects of charge separation in bacterial photosynthesis: theoretical models. *J. Am. Chem. Soc.* **1987**, *109* (15), 4728-4730.

(64) Jiang, X.; Futera, Z.; Blumberger, J. Ergodicity-breaking in thermal biological electron transfer? Cytochrome C revisited. *J. Phys. Chem. B* **2019**, *123* (35), 7588-7598.

(65) Futera, Z.; Jiang, X.; Blumberger, J. Ergodicity breaking in thermal biological electron transfer? Cytochrome C revisited II. *J. Phys. Chem. B* **2020**, *124* (16), 3336-3342.

(66) Bradshaw, R. T.; Dziedzic, J.; Skylaris, C.-K.; Essex, J. W. The role of electrostatics in enzymes: do biomolecular force fields reflect protein electric fields? *J. Chem. Inf. Model.* **2020**, *60* (6), 3131-3144.

(67) Jiang, X.; Futera, Z.; Ali, M. E.; Gajdos, F.; von Rudorff, G. F.; Carof, A.; Breuer, M.; Blumberger, J. Cysteine Linkages Accelerate Electron Flow through Tetra-Heme Protein STC. *J. Am. Chem. Soc.* **2017**, *139* (48), 17237-17240. DOI: 10.1021/jacs.7b08831 From NLM Medline.

(68) van Wonderen, J. H.; Adamczyk, K.; Wu, X.; Jiang, X.; Piper, S. E. H.; Hall, C. R.; Edwards, M. J.; Clarke, T. A.; Zhang, H.; Jeuken, L. J. C.; et al. Nanosecond heme-to-heme electron transfer rates in a multiheme cytochrome nanowire reported by a spectrally unique His/Met-ligated heme. *Proc. Natl. Acad. Sci. U. S. A.* **2021**, *118* (39). DOI: 10.1073/pnas.2107939118 From NLM Medline.

(69) van Wonderen, J. H.; Hall, C. R.; Jiang, X.; Adamczyk, K.; Carof, A.; Heisler, I.; Piper, S. E. H.; Clarke, T. A.; Watmough, N. J.; Sazanovich, I. V.; et al. Ultrafast Light-Driven Electron Transfer in a Ru(II)tris(bipyridine)-Labeled Multiheme Cytochrome. *J. Am. Chem. Soc.* **2019**, *141* (38), 15190-15200. DOI: 10.1021/jacs.9b06858 From NLM Medline.

(70) Blumberger, J. Free energies for biological electron transfer from QM/MM calculation: method, application and critical assessment. *Phys. Chem. Chem. Phys.* **2008**, *10* (37), 5651-5667.

(71) Smith, D. M.; Rosso, K. M.; Dupuis, M.; Valiev, M.; Straatsma, T. Electronic coupling between heme electron-transfer centers and its decay with distance depends strongly on relative orientation. *J. Phys. Chem. B* **2006**, *110* (31), 15582-15588.

(72) Jiang, X.; Burger, B.; Gajdos, F.; Bortolotti, C.; Futera, Z.; Breuer, M.; Blumberger, J. Kinetics of trifurcated electron flow in the decaheme bacterial proteins MtrC and MtrF. *Proc. Natl. Acad. Sci. U. S. A.* **2019**, *116* (9), 3425-3430. DOI: 10.1073/pnas.1818003116 From NLM Medline.

(73) Sigfridsson, E.; Olsson, M. H.; Ryde, U. A comparison of the inner-sphere reorganization energies of cytochromes, iron− sulfur clusters, and blue copper proteins. *J. Phys. Chem. B* **2001**, *105* (23), 5546-5552.

(74) Amashukeli, X.; Gruhn, N. E.; Lichtenberger, D. L.; Winkler, J. R.; Gray, H. B. Inner-sphere electron-transfer reorganization energies of zinc porphyrins. *J. Am. Chem. Soc*. **2004**, *126* (47), 15566-15571.

(75) Tipmanee, V.; Oberhofer, H.; Park, M.; Kim, K. S.; Blumberger, J. Prediction of reorganization free energies for biological electron transfer: A comparative study of Ru-modified cytochromes and a 4-helix bundle protein. *J. Am. Chem. Soc.* **2010**, *132* (47), 17032-17040.

(76) Page, C. C.; Moser, C. C.; Chen, X.; Dutton, P. L. Natural engineering principles of electron tunnelling in biological oxidation–reduction. *Nature* **1999**, *402* (6757), 47-52.

(77) Alvarez-Paggi, D.; Castro, M. A.; Tórtora, V.; Castro, L.; Radi, R.; Murgida, D. H. Electrostatically driven second-sphere ligand switch between high and low reorganization energy forms of native cytochrome c. *J. Am. Chem. Soc.* **2013**, *135* (11), 4389-4397.

(78) Chattopadhyay, S.; Mukherjee, M.; Kandemir, B.; Bowman, S. E.; Bren, K. L.; Dey, A. Contributions to cytochrome c inner-and outer-sphere reorganization energy. *Chem. Sci.* **2021**, *12* (35), 11894-11913.

(79) Derrida, B. Velocity and diffusion constant of a periodic one-dimensional hopping model. *J. Stat. Phys.* **1983**, *31*, 433-450.

(80) Cahen, D.; Pecht, I.; Sheves, M. What Can We Learn from Protein-Based Electron Transport Junctions? *J. Phys. Chem. Lett.* **2021**, *12* (47), 11598-11603. DOI: 10.1021/acs.jpclett.1c02446 From NLM Medline.

(81) Guberman-Pfeffer, M. J. Analysis programs used for the article Five Cytochrome 'Nanowires' Suffice for Prokaryotes to Breathe Rocks Microns Away. **2024**. Zenodo.

(82) Karnaukh, E. A.; Bravaya, K. B. The redox potential of a heme cofactor in Nitrosomonas europaea cytochrome c peroxidase: A polarizable QM/MM study. *Phys. Chem. Chem. Phys.* **2021**, *23* (31), 16506-16515.

(83) Hornak, V.; Abel, R.; Okur, A.; Strockbine, B.; Roitberg, A.; Simmerling, C. Comparison of multiple Amber force fields and development of improved protein backbone parameters. *Proteins: Struct., Funct., Bioinf.* **2006**, *65* (3), 712-725.

(84) Crespo, A.; Martí, M. A.; Kalko, S. G.; Morreale, A.; Orozco, M.; Gelpi, J. L.; Luque, F. J.; Estrin, D. A. Theoretical study of the truncated hemoglobin HbN: exploring the molecular basis of the NO detoxification mechanism. *J. Am. Chem. Soc.* **2005**, *127* (12), 4433-4444.

(85) Henriques, J. o.; Costa, P. J.; Calhorda, M. J.; Machuqueiro, M. Charge Parametrization of the D v H-c 3 Heme Group: Validation Using Constant-(pH, E) Molecular Dynamics Simulations. *J. Phys. Chem. B* **2013**, *117* (1), 70-82.

(86) Jorgensen, W. L.; Chandrasekhar, J.; Madura, J. D.; Impey, R. W.; Klein, M. L. Comparison of simple potential functions for simulating liquid water. *J. Chem. Phys.* **1983**, *79* (2), 926-935.

(87) Joung, I. S.; Cheatham III, T. E. Determination of alkali and halide monovalent ion parameters for use in explicitly solvated biomolecular simulations. *J. Phys. Chem. B* **2008**, *112* (30), 9020-9041.

(88) Lee, C.; Yang, W.; Parr, R. Density-functional exchange-energy approximation with correct asymptotic behaviour. *Phys. Rev. B* **1988**, *37* (2), 785.

(89) Beck, A. D. Density-functional thermochemistry. III. The role of exact exchange. *J. Chem. Phys.* **1993**, *98* (7), 5648-5646.

(90) Stephens, P. J.; Devlin, F. J.; Chabalowski, C. F.; Frisch, M. J. Ab initio calculation of vibrational absorption and circular dichroism spectra using density functional force fields. *J. Phys. Chem.* **1994**, *98* (45), 11623-11627.

(91) Hay, P. J.; Wadt, W. R. Ab initio effective core potentials for molecular calculations. Potentials for K to Au including the outermost core orbitals. *J. Chem. Phys.* **1985**, *82* (1), 299-310.

(92) Roy, L. E.; Hay, P. J.; Martin, R. L. Revised basis sets for the LANL effective core potentials. *J. Chem. Theory Comput.* **2008**, *4* (7), 1029-1031.

(93) Francl, M. M.; Pietro, W. J.; Hehre, W. J.; Binkley, J. S.; Gordon, M. S.; DeFrees, D. J.; Pople, J. A. Self□consistent molecular orbital methods. XXIII. A polarization□type basis set for second□row elements. *J. Chem. Phys.* **1982**, *77* (7), 3654-3665.

(94) Krishnan, R.; Binkley, J. S.; Seeger, R.; Pople, J. A. Self□consistent molecular orbital methods. XX. A basis set for correlated wave functions. *J. Chem. Phys.* **1980**, *72* (1), 650-654.

(95) McLean, A.; Chandler, G. Contracted Gaussian basis sets for molecular calculations. I. Second row atoms, Z= 11–18. *J. Chem. Phys.* **1980**, *72* (10), 5639-5648.

(96) *Gaussian 16 Rev. A.03*; Wallingford, CT, 2016. (accessed.

(97) Case, D. A.; Aktulga, H. M.; Belfon, K.; Cerutti, D. S.; Cisneros, G. A.; Cruzeiro, V. W. D.; Forouzesh, N.; Giese, T. J.; Go□tz, A. W.; Gohlke, H. AmberTools. *J. Chem. Theory Comput.* **2023**, *63* (20), 6183-6191.